Acta Crystallographica Section F
Structural Biology and Crystallization Communications
ISSN 1744-3091

Crystallization and preliminary X-ray analysis of the N-terminal domain of human thioredoxin-interacting protein

Galina Polekhina,[a]* David Benjamin Ascher,[b] Shie Foong Kok[a] and Mark Waltham[c]

[a]Structural Biology, Monash Institute of Medical Research, Monash University, 27–31 Wright Street, Clayton, Victoria 3168, Australia, [b]Structural Biology, St Vincent's Institute of Medical Research, 9 Princes Street, Fitzroy, Victoria 3065, Australia, and [c]Pharmacogenomics Unit, St Vincent's Institute of Medical Research, 9 Princes Street, Fitzroy, Victoria 3065, Australia

Correspondence e-mail: galina.polekhina@monash.edu

Received 20 February 2011
Accepted 18 March 2011

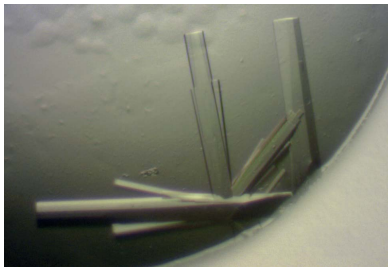

Thioredoxin-interacting protein (TXNIP) is a negative regulator of thioredoxin and its roles in the pathologies of diabetes and cardiovascular diseases have marked it out as a potential drug target. Expression of TXNIP is robustly induced under various stress conditions such as high glucose, heat shock, UV, H_2O_2 and mechanical stress amongst others. Elevated levels of TXNIP result in the sequestration and inactivation of thioredoxin, leading to cellular oxidative stress. For some time, this was the only known function of TXNIP; however, more recently the protein has been shown to play a role in regulation of glucose uptake and activation of the inflammasome. Based on the primary sequence, TXNIP is remotely related to β-arrestins, which include the visual arrestins. TXNIP has thus been classified as a member of the α-arrestin family, which to date includes five other members. None of the other α-arrestins are known to interact with thioredoxin, although curiously one has been implicated in glucose uptake. In order to gain insight into the structure–function relationships of the α-arrestin protein family, and particularly that of TXNIP, the N-terminal domain of TXNIP has been crystallized. The crystals belonged to a monoclinic space group and diffracted to 3 Å resolution using synchrotron radiation.

1. Introduction

Thioredoxin-interacting protein (TXNIP), which is also known as thioredoxin-binding protein 2 (TBP-2) and vitamin D-upregulated protein 1 (VDUP-1), has been identified as a binding partner of thioredoxin (TRX) *via* a yeast two-hybrid system (Junn *et al.*, 2000; Nishiyama *et al.*, 1999). Stress stimuli including high glucose, UV, H_2O_2, heat shock and mechanical stress amongst others robustly induce TXNIP expression, while the expression and protein levels of TRX remain the same or are down-regulated under at least some of these conditions (Nishiyama *et al.*, 1999; Schulze *et al.*, 2004). The association of TXNIP and TRX leads to inhibition of TRX activity, resulting in oxidative stress (Schulze *et al.*, 2004), and also impacts on the many different cellular processes regulated by TRX (Kaimul *et al.*, 2007). The active-site cysteines of TRX, Cys32 and Cys35, in their reduced states are important for mediating the interaction with TXNIP (Nishiyama *et al.*, 1999). Cys247 and Cys63 of TXNIP, which are proposed to be involved in the intramolecular disulfide bond, have been implicated in interaction with TRX (Patwari *et al.*, 2006). Cys247 has been shown to be essential for interaction, while Cys63 has been shown to be important for efficient binding. If TRX reduces the intramolecular disulfide bond between Cys63 and Cys247 of TXNIP then TXNIP is a substrate of TRX. However, this would contradict the role of TXNIP as an inhibitor of thioredoxin, as the TXNIP–TRX complex does not disassociate following the reduction of the intramolecular disulfide bond as would be expected for a normal substrate.

Several recent gene-array studies on human and rat islets have identified TXNIP as one of the most dramatically glucose-induced genes in insulin resistance/diabetes (Minn *et al.*, 2005; Oka *et al.*, 2009; Qi *et al.*, 2007). Elevated expression of TXNIP has also been shown to contribute to pathologies in diabetes (Kobayashi *et al.*, 2003; Qi *et al.*, 2009). TXNIP's pro-apoptotic effects on beta cells provide a possible link between glucose toxicity and beta-cell death (Chen, Saxena *et al.*,

2008; Shalev, 2008). The use of HcB-19 mice containing a nonsense mutation in TXNIP that eliminates its expression, as well as TXNIP knockout mice and beta-cell specific knockouts, have consistently highlighted the roles of TXNIP in glucose and lipid metabolism (Bodnar *et al.*, 2002; Chen, Hui *et al.*, 2008; Hui *et al.*, 2004). This is consistent with observations that a lack of TXNIP protects against diabetes (Shalev, 2008). Indeed, it was subsequently shown that TXNIP is involved in glucose uptake (Patwari *et al.*, 2009). Interestingly, this occurs independently of the ability of TXNIP to bind TRX, as was elegantly established using a TXNIP cysteine mutant unable to bind TRX. Specific TXNIP down-regulation has also been shown to be beneficial during heart ischaemia (Xiang *et al.*, 2005). Thus, disrupting the interaction between TXNIP and TRX might turn out to be therapeutically beneficial in conditions such as diabetes and cardiovascular disease.

More recently, TXNIP has been shown to activate the inflammasome, which is a major player in innate immunity (Zhou *et al.*, 2010). The C-terminal domain of TXNIP has been shown to interact with the NLRP3 component of the inflammasome *via* the C-terminal leucine-rich repeats of NLRP3. Given the role of the inflammasome in maturation of IL-6β and the emerging role of IL-6β in pancreatic islet failure in type 2 diabetes, this reinforces the contribution of TXNIP to pathologies of diabetes.

Based on primary sequence, TXNIP is related to five other genes in the human genome, which are collectively termed α-arrestins (Alvarez, 2008). None of the other five proteins bind TRX and their possible binding partners and physiological roles have yet to be elucidated. α-Arrestins are related to β-arrestins, for which several crystal structures are available (Hirsch *et al.*, 1999; Milano *et al.*, 2002). Owing to the very low (~10%) sequence identity between α-arrestins and β-arrestins it is not possible to construct a molecular model with confidence and several equally plausible sequence alignments can be produced. While the arrestin fold seems to be a mediator of protein–protein interaction, only TRX and the leucine-rich repeats domain of NLRP3 have so far been established as binding partners of TXNIP. Inspection of the primary sequence suggests that although the overall structure of α-arrestin is predicted to be similar to that of β-arrestins, some features of β-arrestins appear not to be present in α-arrestins. While there is evidence that the TRX-binding site is confined to the C-terminal domain of TXNIP, both the N-terminal and the C-terminal domains appear to influence glucose uptake (Patwari *et al.*, 2009). However, the C-terminal tail does not seem to be necessary for either binding of thioredoxin or glucose uptake. Cys63 and Cys247, both of which have been implicated in the interaction with TRX, are located in the N-terminal and C-terminal domains, respectively. Moreover, they are spatially distant in the models that we have constructed and those generated by automatic modelling servers. This poses the question as to whether the intramolecular disulfide bond proposed between Cys63 and Cys247 can exist in TXNIP.

Given the pivotal role of TXNIP in a number of important biological pathways and its potential as a drug target, high-resolution structural information would be of immense value. We have initiated structural studies of TXNIP and its domains in order to shed light on its structure–function relationship and ultimately to determine high-resolution structures of TXNIP and its complex with TRX. Here, we report the crystallization and preliminary X-ray analysis of the N-terminal domain of TXNIP.

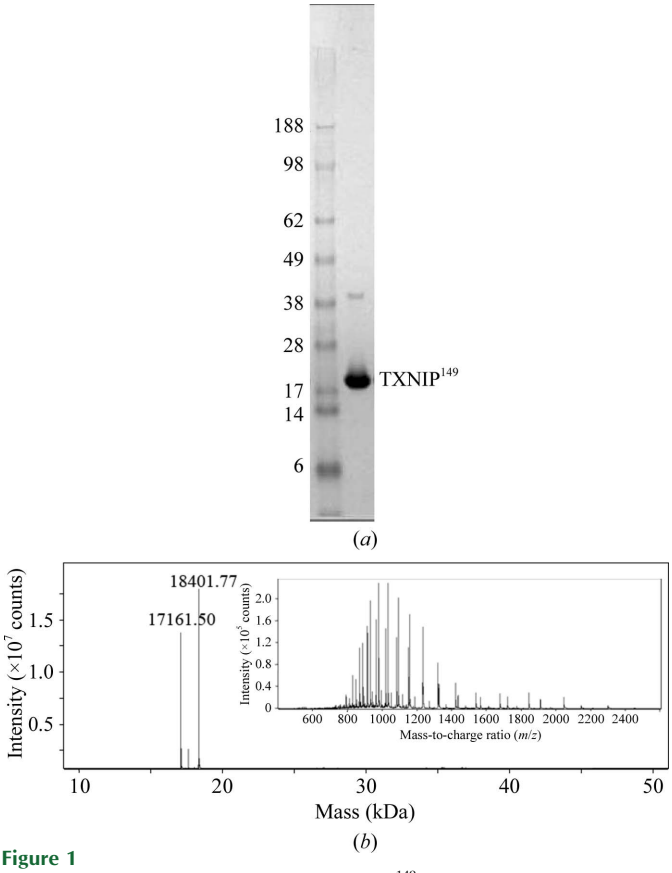

Figure 1
(*a*) 4–12% SDS–PAGE showing purified TXNIP^{149}. Molecular-weight markers are labelled in kDa. (*b*) Deconvoluted ESI–TOF mass spectrum of TXNIP^{161} eluted from Superdex 75; raw MS data plotted as intensity *versus* mass-to-charge ratio are shown in the inset.

2. Experimental procedures and results

2.1. Expression and purification

The N-terminal domain of human TXNIP, initially encompassing residues 1–161 (TXNIP^{161}) and later refined to include residues 1–149 (TXNIP^{149}), was cloned using ligation-independent cloning into a modified pMCSG7 vector (Stols *et al.*, 2002) in which human TRX^{C73S} was inserted into the *Kpn*I site between the His_6 tag and the TEV protease-recognition site to serve as a solubility tag. Human TRX is known to dimerize *via* Cys73 (Weichsel *et al.*, 1996). In TXNIP the cysteine residues 36, 70 and 120 were mutated to serines, but the only other cysteine in this construct, Cys63, was not mutated owing to its reported role in the interaction with TRX. The rationale for mutating the cysteines was to avoid the potential aggregation problems that we have observed during the expression of other TXNIP constructs. Expression and purification of TXNIP^{161} and TXNIP^{149} followed the same protocol. *E. coli* containing the recombinant plasmid was grown in Power Prime Broth (Athena Environmental Biosciences) at 310 K to an optical density of 0.6–0.8 at 600 nm. Expression was then induced by adding IPTG to a final concentration of 0.1 m*M* and culture growth continued at 295 K for 4 h. The bacterial cells were then harvested by centrifugation at 5000*g* for 30 min and the pellets were stored at 253 K until purification.

For lysis, the cells were resuspended in BugBuster Protein Extraction reagent (10 ml per gram of cells; Novagen) supplemented with lysozyme, DNase I, a 1:200 volume ratio of protease-inhibitor cocktail (Sigma) and either 2 m*M* DTT or 20 m*M* β-mercaptoethanol as a reducing agent. The cell suspension was incubated for 30 min at 295 K with gentle rocking and the cell debris and any insoluble material were removed by centrifugation at 25 000*g* for 30 min. The

resulting supernatant was applied onto a HisTrap 5 ml column (GE Healthcare) previously equilibrated with 20 m*M* sodium phosphate buffer pH 7.4, 0.5 *M* NaCl, 20 m*M* imidazole. The column was washed with the same buffer and the protein of interest was eluted with either a continuous or a stepwise gradient of imidazole to 350 m*M*. The fractions containing His_6-hTRX^{C73S}-TEV-TXNIP were pooled and dialysed overnight against 20 m*M* sodium phosphate buffer pH 7.4, 0.5 *M* NaCl, 1 m*M* DTT (or 20 m*M* β-mercaptoethanol) at 277 K. TEV protease was added to the dialysed sample in a 1:100 ratio to cleave the purification/solubility tag from TXNIP and the mixture was incubated at 295 K for the first 6–8 h and at 277 K for a further 10–12 h. TXNIP was separated from His_6-hTRX^{C73S} and TEV by applying it onto a HisTrap column and collecting the flowthrough fractions. TXNIP was then concentrated and purified further using a Superdex 75 HiLoad 26/60 column (GE Healthcare) using a buffer consisting of 25 m*M* Tris pH 7.5, 150 m*M* NaCl, 1 m*M* DTT (or 20 m*M* β-mercaptoethanol). The fractions containing TXNIP were pooled and concentrated using an Amicon-15 10K molecular-weight cutoff (MWCO) concentrator. NaCl was removed from the sample using an NAP-25 column (GE Healthcare). The purified protein was again concentrated using an Amicon-4 10K MWCO concentrator to a final concentration of 4–5 mg ml^{-1} for crystallization (Fig. 1*a*).

Previous studies on TXNIP suggested that the TRX-binding site was located in the C-terminal domain (Kobayashi *et al.*, 2003; Patwari *et al.*, 2006). Our expression construct offered an opportunity to directly test this by running size-exclusion chromatography following the TEV cleavage, when we had a 1:1 mixture of His_6-hTRX^{C73S} and TXNIP^{161}. Indeed, the N-terminal domain of TXNIP does not bind TRX on its own as His_6-hTRX^{C73S} and TXNIP^{161} eluted as two separate peaks.

2.2. Mass spectrometry

During the purification of TXNIP^{161}, we noticed that the TEV cleavage was producing two TXNIP species with an approximately 2 kDa difference in molecular weight. Although the two species eluted as a single peak from the gel filtration, the higher molecular-weight polypeptide, which we assumed at this stage to be TXNIP^{161}, could be predominantly separated from the lower molecular-weight species by collecting the earlier eluting fractions from the gel filtration. However, it is most likely that owing to the small difference in size the protein sample contains a combination of protein species, which may be disadvantageous for crystallization and detrimental to the quality of crystals. We therefore employed mass spectrometry (MS) to precisely identify the nature of the two fragments. MS was performed using an Agilent Q-Tof LC/MS with a C8 column and a gradient of 5–75% acetonitrile in 0.1% formic acid. This identified the molecular weights of the two species as 18 401.77 and 17 161.5 (Fig. 1*b*). The first mass corresponds to the theoretical mass 18 325.83 of TXNIP^{161} as an adduct with β-mercaptoethanol, which was used during purification in this instance. The second mass corresponds to the theoretical mass 17 085.44 of TXNIP^{149}, also as an adduct with β-mercaptoethanol. We therefore shortened our construct for the N-terminal domain to include residues 1–149 of TXNIP in order to avoid potentially having a mixture of two samples in crystallization.

Table 1
Diffraction data statistics.

Values in parentheses are for the highest resolution shell.

Space group	$P2_1$
Unit-cell parameters (Å, °)	a = 79, b = 179, c = 88, α = 90, β = 113, γ = 90
Wavelength (Å)	0.95374
Resolution range (Å)	56.5–2.99 (3.15–2.99)
Total observations	323180 (47676)
Unique reflections	42272 (6205)
Multiplicity	7.6 (7.7)
Completeness (%)	100.0 (100.0)
Mean $I/\sigma(I)$	15.4 (2.9)
R_{merge} (%)	9.5 (76.9)

2.3. Crystallization

Initial crystallization screening was performed on TXNIP^{161} at the Bio21 Collaborative Crystallization Center (C^3; http://www.csiro.au/c3/). Over 1500 conditions were trialled. Two conditions produced small needle-like crystals: 0.2 *M* $CaCl_2$, 20%(*w*/*v*) PEG 3350, 0.02% NaN_3 and 0.2 *M* $CaCl_2$, 20%(*w*/*v*) PEG 6000, 0.1 *M* HEPES pH 7.0, 0.02% NaN_3. The crystals diffracted to approximately 4.5 Å resolution using our in-house MicroMax-007 X-ray source. Screening was also performed on TXNIP^{149}, but did not identify any alternative crystallization conditions.

Through refinement, the optimal crystallization conditions for TXNIP^{149} were defined as 0.1 *M* HEPES pH 7.5, 0.2 *M* calcium acetate, 10–12%(*w*/*v*) PEG monomethyl ether 5000 (Fig. 2). The crystals grew at 295 K using the hanging-drop vapour-diffusion method, reaching typical dimensions of 0.05–0.1 × 0.05–0.1 × 0.2–0.5 mm over three weeks.

2.4. Data collection and preliminary X-ray analysis

Crystals were flash-frozen after stepwise transfer into the final cryobuffer. Glycerol was used as a cryoprotectant and was added in

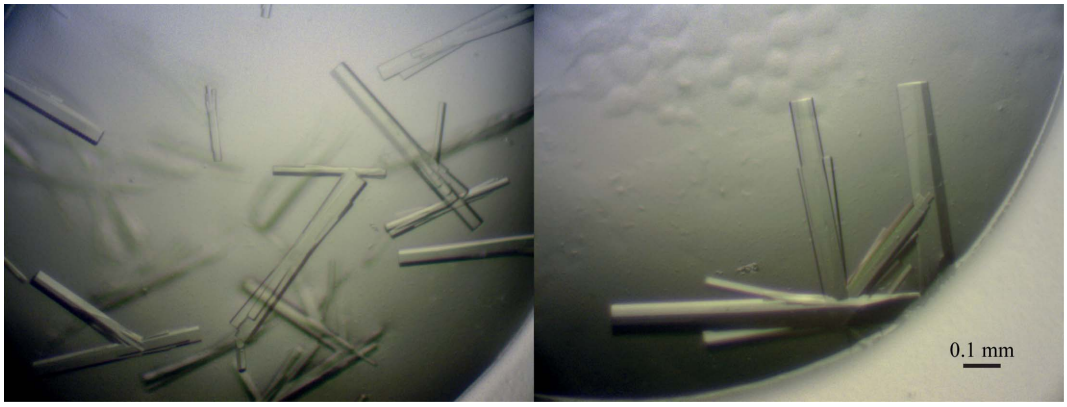

Figure 2
Crystals of TXNIP^{149} grown in 0.1 *M* HEPES pH 7.5, 0.2 *M* calcium acetate, 10–12%(*w*/*v*) PEG monomethyl ether 5000.

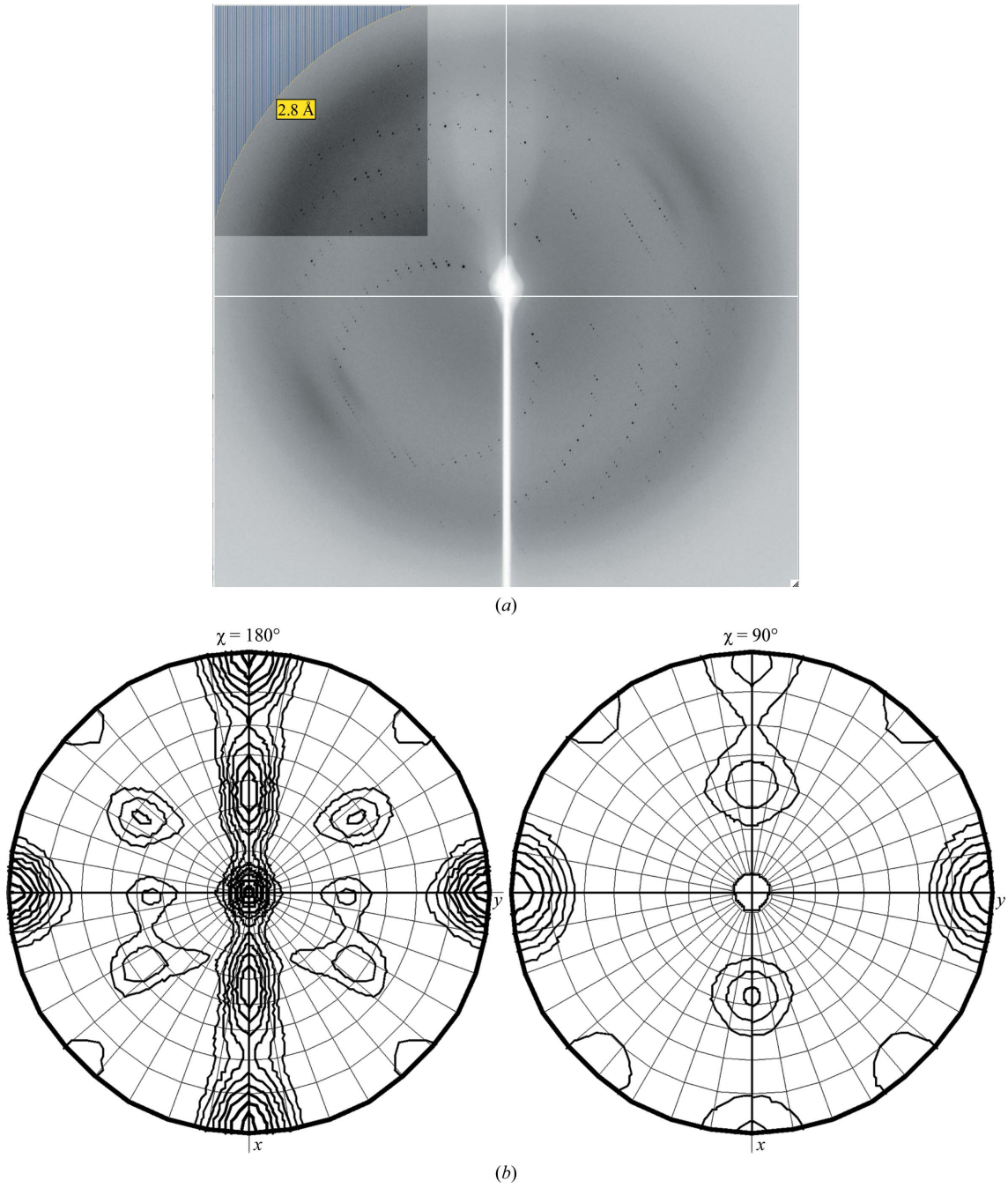

Figure 3
(*a*) X-ray diffraction pattern recorded from a TXNIP[149] crystal on beamline MX1 at the Australian Synchrotron. (*b*) The self-rotation function calculated to a resolution of 6 Å.

steps of 5%(*v*/*v*) up to 15 or 20%(*v*/*v*) to stabilizing buffer consisting of 0.1 m*M* HEPES pH 7.5, 0.2 *M* calcium acetate, 15%(*w*/*v*) PEG monomethyl ether 5000. The higher concentration (20%) of the cryoprotectant was used for larger crystals. The soaking time for each step was 2–3 min. A complete data set was collected using an ADSC Q210 detector on the MX1 beamline at the Australian synchrotron (McPhillips *et al.*, 2002). The crystals diffracted to approximately 3 Å resolution (Fig. 3*a*) and belonged to the monoclinic space group *P*2 or $P2_1$, with unit-cell parameters $a = 79$, $b = 179$, $c = 88$ Å, $\beta = 113^\circ$. The odd reflections along 0*k*0 were absent, unequivocally indicating the presence of a screw axis and thus identifying $P2_1$ as the correct space group. The data were processed using *MOSFLM* (Leslie, 1992) and were scaled using the program *SCALA* from the *CCP*4 suite (Winn *et al.*, 2011). The X-ray data statistics are shown in Table 1. The calculated Matthews coefficient (V_M) of 31.16 Å^3 Da^{-1} for the asymmetric unit suggests the possible presence of at least eight and as many as 12 molecules per asymmetric unit, corresponding to a solvent content of 50–70% (Matthews, 1968). A native Patterson map did not reveal any significant peaks and therefore no translational symmetry is present in the crystal. A self-rotation function calculated using *MOLREP* (Vagin & Teplyakov, 2010) in various resolution ranges identified several twofold axes perpendicular to the crystallographic twofold axis and possibly a fourfold axis coinciding with the crystallographic 2_1 axis (Fig. 3*b*). The crystal structures of several β-arrestins as well as

theoretical models of TXNIP are available for use in molecular replacement.

GP is a recipient of a Career Development Award from the National Health and Medical Research Council (NHMRC) of Australia. This work was also supported by a grant from NHMRC to GP and MW. DBA was an Australian Postgraduate Award Scholar and a recipient of a St Vincent's Institute Foundation Scholarship sponsored by Colin North and Major Engineering. This research was undertaken at the Australian Synchrotron, Victoria, Australia. We appreciate the support provided by all staff at the Australian synchrotron during our visits. We would also like to acknowledge the staff and particularly Dr Janet Newman at the Bio21 Collaborative Crystallographic Centre at CSIRO Molecular and Health Technologies, Parkville, Melbourne.

References

Alvarez, C. E. (2008). *BMC Evol. Biol.* **8**, 222.
Bodnar, J. S. *et al.* (2002). *Nature Genet.* **30**, 110–116.
Chen, J., Hui, S. T., Couto, F. M., Mungrue, I. N., Davis, D. B., Attie, A. D., Lusis, A. J., Davis, R. A. & Shalev, A. (2008). *FASEB J.* **22**, 3581–3594.
Chen, J., Saxena, G., Mungrue, I. N., Lusis, A. J. & Shalev, A. (2008). *Diabetes*, **57**, 938–944.
Hirsch, J. A., Schubert, C., Gurevich, V. V. & Sigler, P. B. (1999). *Cell*, **97**, 257–269.
Hui, T. Y., Sheth, S. S., Diffley, J. M., Potter, D. W., Lusis, A. J., Attie, A. D. & Davis, R. A. (2004). *J. Biol. Chem.* **279**, 24387–24393.
Junn, E., Han, S. H., Im, J. Y., Yang, Y., Cho, E. W., Um, H. D., Kim, D. K., Lee, K. W., Han, P. L., Rhee, S. G. & Choi, I. (2000). *J. Immunol.* **164**, 6287–6295.
Kaimul, A. M., Nakamura, H., Masutani, H. & Yodoi, J. (2007). *Free Radic. Biol. Med.* **43**, 861–868.
Kobayashi, T., Uehara, S., Ikeda, T., Itadani, H. & Kotani, H. (2003). *Kidney Int.* **64**, 1632–1642.
Leslie, A. G. W. (1992). *Jnt CCP4/ESF–EACBM Newsl. Protein Crystallogr.* **26**.
Matthews, B. W. (1968). *J. Mol. Biol.* **33**, 491–497.
McPhillips, T. M., McPhillips, S. E., Chiu, H.-J., Cohen, A. E., Deacon, A. M., Ellis, P. J., Garman, E., Gonzalez, A., Sauter, N. K., Phizackerley, R. P., Soltis, S. M. & Kuhn, P. (2002). *J. Synchrotron Rad.* **9**, 401–406.
Milano, S. K., Pace, H. C., Kim, Y. M., Brenner, C. & Benovic, J. L. (2002). *Biochemistry*, **41**, 3321–3328.
Minn, A. H., Hafele, C. & Shalev, A. (2005). *Endocrinology*, **146**, 2397–2405.
Nishiyama, A., Matsui, M., Iwata, S., Hirota, K., Masutani, H., Nakamura, H., Takagi, Y., Sono, H., Gon, Y. & Yodoi, J. (1999). *J. Biol. Chem.* **274**, 21645–21650.
Oka, S., Yoshihara, E., Bizen-Abe, A., Liu, W., Watanabe, M., Yodoi, J. & Masutani, H. (2009). *Endocrinology*, **150**, 1225–1234.
Patwari, P., Chutkow, W. A., Cummings, K., Verstraeten, V. L., Lammerding, J., Schreiter, E. R. & Lee, R. T. (2009). *J. Biol. Chem.* **284**, 24996–25003.
Patwari, P., Higgins, L. J., Chutkow, W. A., Yoshioka, J. & Lee, R. T. (2006). *J. Biol. Chem.* **281**, 21884–21891.
Qi, W., Chen, X., Gilbert, R. E., Zhang, Y., Waltham, M., Schache, M., Kelly, D. J. & Pollock, C. A. (2007). *Am. J. Pathol.* **171**, 744–754.
Qi, W., Chen, X., Holian, J., Tan, C. Y., Kelly, D. J. & Pollock, C. A. (2009). *Am. J. Pathol.* **175**, 1858–1867.
Schulze, P. C., Yoshioka, J., Takahashi, T., He, Z., King, G. L. & Lee, R. T. (2004). *J. Biol. Chem.* **279**, 30369–30374.
Shalev, A. (2008). *Biochem. Soc. Trans.* **36**, 963–965.
Stols, L., Gu, M., Dieckman, L., Raffen, R., Collart, F. R. & Donnelly, M. I. (2002). *Protein Expr. Purif.* **25**, 8–15.
Vagin, A. & Teplyakov, A. (2010). *Acta Cryst.* D**66**, 22–25.
Weichsel, A., Gasdaska, J. R., Powis, G. & Montfort, W. R. (1996). *Structure*, **4**, 735–751.
Winn, M. D. *et al.* (2011). *Acta Cryst.* D**67**, 235–242.
Xiang, G., Seki, T., Schuster, M. D., Witkowski, P., Boyle, A. J., See, F., Martens, T. P., Kocher, A., Sondermeijer, H., Krum, H. & Itescu, S. (2005). *J. Biol. Chem.* **280**, 39394–39402.
Zhou, R., Tardivel, A., Thorens, B., Choi, I. & Tschopp, J. (2010). *Nature Immunol.* **11**, 136–140.